IEEE Access
Multidisciplinary | Rapid Review | Open Access Journal

Received 31 August 2022, accepted 17 September 2022, date of publication 22 September 2022,
date of current version 30 September 2022.

Digital Object Identifier 10.1109/ACCESS.2022.3208883

RESEARCH ARTICLE

Tactile Resilience of Sensory Whisker by Adaptive Morphology

NHAN HUU NGUYEN[1], (Member, IEEE), HELMUT HAUSER[2,3], (Member, IEEE), PERLA MAIOLINO[4], (Member, IEEE), AND VAN ANH HO[1,5], (Senior Member, IEEE)

[1]Soft Haptics Laboratory, Japan Advanced Institute of Science and Technology, Nomi, Ishikawa 923-1292, Japan
[2]Department of Engineering Mathematics, University of Bristol, BS8 1TW Bristol, U.K.
[3]SoftLab, Bristol Robotics Laboratory, BS16 1QY Bristol, U.K.
[4]Oxford Robotics Institute, University of Oxford, OX1 3PJ Oxford, U.K.
[5]Japan Science and Technology Agency, PRESTO, Kawaguchi, Saitama 332-0012, Japan

Corresponding author: Van Anh Ho (van-ho@jaist.ac.jp)

This work was fully supported by the Japan Society for the Promotion of Science (JSPS) Grant-in-Aid for Scientific Research KAKENHI 21H01287 and partly supported by the Engineering and Physical Sciences Research Council (EPSRC) grant EP/V000748/1.

ABSTRACT Nature is featured by the resiliency, which enables adaptivity to sudden change under many circumstances. Meanwhile, the resiliency in robotic systems is far from comparable to that of the nature. If a robot is partially damaged, often the whole system fails to operate properly. While some approaches have been proposed, the majority of them are focusing on updating the control policy. Such approach, while rather complex, is not always applicable to mechanical damage of the robot body, especially parts that continuously interact with the surrounding environment. In the previous works Nguyen and Ho, (2022) and Nguyen and Ho, (2021) we introduced an artificial whiskered sensor that exhibited resilience against physical damage by active change of its morphology around the placement of sensory elements (strain gauges), which allowed compensation of location sensing when the whisker was trimmed. In this paper, we extend the approach by using the whisker sensor for texture discrimination tasks. We demonstrate that changing the morphology of the whisker again helps to reduce mismatching between prior knowledge in the frequency/time domain of the sensory signal. This allows the sensory whisker to recover the tactile perception on texture discrimination after the whisker is partially damaged. Furthermore, we also observe that using adaptive sensor morphology would augment tactile perception without the need of computationally expensive recognition and re-classification. This work is expected to shed a light on a new generation of robots that automatically work in the open world where self-maintenance against uncertainties is needed.

INDEX TERMS Adaptive morphology, augmented tactile perception, morphological computation, tactile compensation, whisker tactile sensor.

NOMENCLATURE

$\boldsymbol{C}$	One-hot vector used for categorizing a specific texture.
WD	Width×Distance index for a texture.
H	Height index for a texture.
RTP	Metrics for evaluating reliability of texture prediction.
$\boldsymbol{\Psi}$	Multi-output vector for texture classifier including $\boldsymbol{C}$, WD and H.
S1, S2	Strain gauge 1 and Strain gauge 2.
SC	Spectrum centroid of a band-pass filtered signal.
TP	Total power of band-pass filtered signal.
PF	Predominant frequency of a band-pass filtered signal.
$\boldsymbol{\Gamma}$	Vector containing texture features.
PM, APM	Positive maximum peaks of a time-series signals and their averages.
Q_{init}, Q_c, Q_u	Pressure value in the air chamber of the whisker's initial, compensated and unknown-predicting states.

The associate editor coordinating the review of this manuscript and approving it for publication was Tao Wang.

ϵ, ϵ_b	Strain gauge responses of whisker's original and broken states.
ϵ^e, ϵ^u	Strain gauge responses perceived from existed and unknown texture.
Δ	Trimmed length of the whisker body.
a	Ratio of contact position with respect to whisker body length.
δ	Deflection of the whisker body measured at the contact spot.
E	Young's modulus.
$\kappa, \delta_{1,2,3}$	Geometrical parameters derived from whisker structure.

I. INTRODUCTION

There is a long standing history of artificial computing machines ranging from Antikythera mechanism of the Ancient Greeks, to the famous Turing machine - the foundation of modern computers [3]. In general, these systems leverage a basic medium (such as mechanical parts, electrical circuits and more recently optical waves [4] or DNA molecules [5]) as computation means for implementing relations of inputs and outputs. Similarly, morphological characteristics in biological systems are well recognized by cognitive [6] and biomimetic [7] scientists to implement computation tasks - widely known as Morphological Computation (MC). Such features not only facilitate interaction with the environment but also, during this process, serve as an architecture based on intrinsic properties (e.g., material stiffness) and structural configuration, where information transmission and processing are performed simultaneously. This allows animals, even primitive ones with deficient nervous systems, to continuously adapt their functionalities to unstructured real-world scenarios [7].

Motivated by the above observations, there have been increasing efforts to exploit the versatility of morphology for engineering intelligent abilities in artificial robotic applications such as locomotion [8], tactile sensing [9], and control [10]. Owing to advances in additive manufacturing, functional material and recent emergence of soft robotics, MC has been widely elaborated. However, current exploitation of MC is still far from its potential. According to literature to date, soft tactile sensors apparently stand as one of the most benefited from MC since their sensing function is generally embodied through their morphological properties. For example, Ho *et al.* [11] demonstrates a multi-modal tactile sensor can be achieved by switching the morphology from one to another. A similar attempt was done by Nurzaman *et al.* [12] where different physical quantities (e.g., softness and temperature) were obtained separately thanks to adjustable sensor morphology. Highly non-linear characteristic of materials commonly used in soft bodies (e.g., silicone rubber) under different levels of external stress excitation is effectively employed to amplify tactile response [13], [14]. Interestingly, the sensor morphology is not only the characteristics of the body alone but combined with other components.

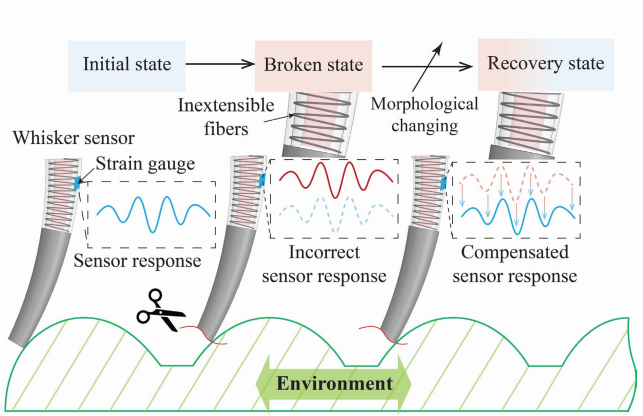

FIGURE 1. Illustration of wrong tactile inference for discrimination tasks due to physical damages and our proposed solution for tactile resilience via adaptive morphology [1], [2].

The placement of sensing elements in the body layout is similar to the interface between mechanoreceptors and the environment in living creatures that drives what the sensor perceives [15], [16]. Authors in [17] attempted to alter the layered rubber skin of a vision-based tactile sensor, which contains a number of markers on it, in order to vary the human-robot haptic interaction for control purposes. Hughes *et al.* [18] proposed a changeable jamming-based filter to enhance successful rate of the tactile discrimination task. This work has proposed that, instead of trying to optimize the design in advance, the sensor body should be able to adapt itself continuously and dependently on the sensing task.

Most of the attention to this research area aims to enrich information gain, it is lacking elaboration on how variable morphology can be utilized to remain sensing ability against unexpected damage to the original sensor body (e.g., being broken, eroded). Our previous work [1] tackled this issue on a whiskered tactile sensor. By actively changing the sensor's morphology thanks to air regulation of the embedded air chamber, the tactile information (mechanical strain) perceived by the broken one was compensated to get close to that of the same stimuli before being damaged [2]. In this work, we highlighted the efficiency of such tactile resilience strategy for the contact localization task which is actually an analysis of *quasi-static* deformation between equilibrium states of the whisker-object contact. The performance drop of the broken sensor remains unclear in more complex *dynamic* sensing problems as simply illustrated in Fig. 1. From this perspective, two following research questions will be clarified in this paper:

1) Could adaptive morphology help to recover sensing ability of a broken sensor for texture discrimination task?
2) Could adaptive morphology help to aid tactile perception with uncertainties from environment, for example, geometrical changes or unknown environment?

To address both questions, we aim to train a feature-based texture classifier based on a supervised regression learning

model for the whisker sensor. Then, we in turn sweep our whisker sensor (both intact and broken whiskers) back and forth over different types of textures. Temporal sensor responses (*i.e.,* mechanical strain) during this process will be recorded and fed into the above classifier. Texture prediction results of the broken sensor before and after applying the tactile compensation strategy show that we can rely on the adaptive variation of morphology to significantly recover the discriminability even with a considerable damage level (see Fig. 1). Furthermore, we also proposed a novel approach, in the context of morphological computation, to give a rough estimate of an unknown surface characteristic (*i.e.,* roughness). An effort has recently tackled the same problem by using morphological features of a tapered spring whisker to predict the roughness of unknown terrains [19]. In this study, the proposed approach is based on the effort to calibrate tactile data obtained from a new texture close to that of a known one. We assume that the *difference in morphology* could give a hint to the *difference in roughness* between two textures. This could augment trained tactile perception in real-time with limited usage of computation sources for online training and recognition.

II. TACTILE COMPENSATION VIA ADAPTIVE MORPHOLOGY

A. INSPIRATION FROM NATURE PERSPECTIVE

The proposed approach was mainly inspired by tactile sensing organs in living creatures such as rats, which play a vital role in collecting essential informative cues from the environment through continuous interaction. Thus, structural damage is unavoidable. To deal with such circumstances (whether temporary during regrow or permanent), instead of completely relying on the central nervous system, animals tend to allow also their sensing organs to adapt by altering morphology. Such recovery ability was observed in, e.g., spider leg, thanks to morphological change of *Lyriform* organs, which act as mechanoreceptors at leg joints [20], [21]. Such research indicated the morphological computation role of Lyriform, which is actually sensible to strain and vibration. In detail, it is speculated that the shape of Lyriform organs changed so that resulted feedback of the broken leg facilitates the neural system (*i.e.,* the brain) to justify the performance in comparison to the original leg. Rodent's vibrissae system exposes a similar phenomenon. A region in the brain called Barrel cortex allocated to the damaged whisker will be shrunk in shape to reduce its sensitivity, while the contrary (*i.e.,* sensitivity increase) will happen to neighbor whiskers to allow them to take over the sensing task temporarily [22].

The above biological observation suggests that a computation process in controller can also be successfully accomplished by adaptable mechanical systems. We previously transferred this idea into an artificial whiskered sensory system as presented in Fig. 2. The whisker body and an air chamber housed inside are tapered with the same inclined angle. Two inextensible fibers are wound helically around

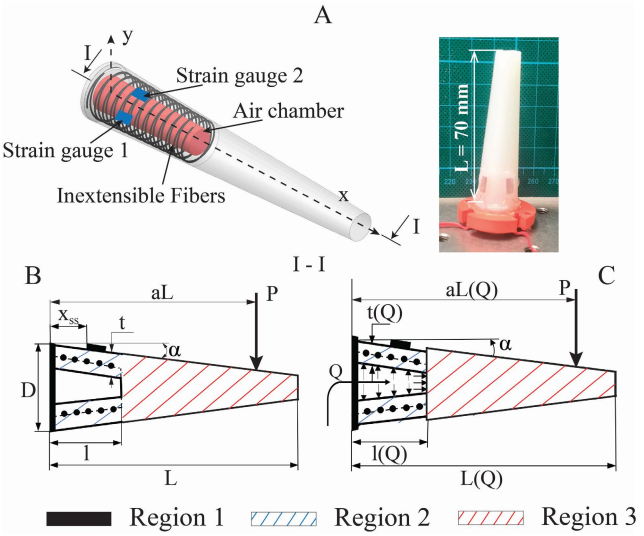

FIGURE 2. (A) Design illustration of our artificial whisker sensor and its capability to enable morphology transformation from chamber-unpressurized state (B) to chamber-pressurized states (C).

the chamber's middle wall to allow only axial length extension (*i.e.,* in x-direction) of the chamber region under inner compressed air Q of the chamber. Two strain gauges (S1 and S2) are bonded onto the chamber region so that their principal sensing planes are perpendicular one to another. By increasing the air pressure Q, the chamber wall will be stiffened. As a consequence, mechanical responses measured by strain gauge are expected to be tuned appropriately to aid sensing capabilities (classification in particular) even with a damaged structure.

B. ANALYTICAL FOUNDATION

A comprehensive understanding of the correlation between sensor morphology (both geometrical and material aspects) and the robotic device outcome is crucial to establishing a proper tactic for damage compensation. In this regard, we previously introduced an analytical model that estimates the strain gauge output for a wide range of contact conditions and morphology states [1]. Based on this, an optimized whisker's layout (upon pressure Q) equivalent to the desired sensitivity is chosen to perform the tactile compensation task. A physics engine based on FE was used to prove that job could be accomplished with high accuracy [2]. A brief derivation of the model is introduced below. For the detail, please refer to [2]

The model leverages two classical beam theories: Hooke's laws and Castigliano's theorem, for the derivation of mechanical strain ε generated due to a certain applied stress σ:

$$\varepsilon = \frac{\sigma}{E_2} = \frac{yM(x)}{E_2 I_2(x)}, \tag{1}$$

where σ is applied stress generated in whisker body due to pure bending moment $M(x)$, y is the radius of the outermost layer of the chamber's wall where the strain gauge is attached. The final expression is:

$$\varepsilon = \frac{4P}{E_2 \pi}\kappa, \tag{2}$$

where κ is a function that is ascribed to the contribution of geometrical parameters (illustrated in Fig. 2) at each equilibrium state of the whisker body. Its expression can be fully reviewed in [1]. In the meantime, the second law is used to describe body's deflection δ by assessing the strain energy stored in each whisker body's region and applying superposition principle in beam deflection:

$$\delta(a) = \frac{\partial U}{\partial P} = \frac{\partial \left(\int_0^{aL} \frac{M(x)^2}{2E_i I_i(x)} dx \right)}{\partial P}, \tag{3}$$

where U is the total strain energy within the body, a is the contact ratio - a coefficient used to generalize the contact distance along the whisker length L: $Contact\ \ distance = a \times L$. The final expression of equation 3 is:

$$\delta(a) = \frac{P}{\pi} \left(\frac{\delta_1}{E_1} + \frac{\delta_2}{E_2} + \frac{\delta_3}{E_3} \right), \tag{4}$$

with δ_i $(i = 1, 2, 3)$ indicates the contribution of geometrical parameters of the region i to total deflection $\delta(a)$ (see full expressions in [1]). Also, $I_i(x)$ and E_i represent the second moment of cross-sectional area and Young's modulus for region i, respectively. Final formulation for the analytical model for the "unpressurized" whisker body is achieved by taking ratio of equation 2 and 4:

$$\frac{\varepsilon}{\delta(a)} = \frac{\kappa}{E_2 \left(\frac{\delta_1}{E_1} + \frac{\delta_2}{E_2} + \frac{\delta_3}{E_3} \right)} = f, \tag{5}$$

and when the chamber is under a certain air pressurization:

$$\frac{\varepsilon(Q)}{\delta(a)} = \frac{\kappa(Q)}{E_2(Q) \left(\frac{\delta_1(Q)}{E_1} + \frac{\delta_2(Q)}{E_2(Q)} + \frac{\delta_3(Q)}{E_3} \right)} = f(Q). \tag{6}$$

Equations 5 and 6 imply two important points. Firstly, any change in either geometrical or material properties (*i.e.,* reflected by $f(Q)$) will result in the variation of sensor response even in a same contact condition. Secondly, we can rely on this model to predict desired morphology state for a certain task, for instance, tactile compensation.

III. METHODOLOGY

This section describes the experimental setup for collecting tactile data, signal decoding and processing the tactile discrimination task. To answer the two aforementioned research questions, our concern is not to distinguish a large number of texture types but just a few with variations in their intrinsic (geometry) parameters. This is expected to clarify the role of sensor morphology in aiding tactile recognition.

A. ARTIFICIAL WHISKER SENSOR AND TEXTURE SAMPLES

We employed the same whisker prototype as in [1] except for an extra strain gauge being used. In detail, S1 plays a major role in generating tactile perception since its sensing plane is coincident with whisker deformation space. Considering the rubbing interaction between a whisker sensor and a textured plate, strain outputs generated by bending deformation are expected to be sufficient to reveal 3-dimensional (3-D) geometry characteristics of the scanned surface. The sensor fabrication is done through a four-step molding process (initially detailed in [1]) using silicon-rubber Dragon Skin 30 (Smooth-On, USA). The strain gauge KFGS-2-120-C1-11 L1M2R (Kyowa, Japan) was used.

TABLE 1. List of textures and their geometrical dimensions.

Index	Texture codes	WD (mm)	H (mm)
1	DB1, HC1, PB1	10	1
2	DB2, HC2, PB2	10	2
3	DB3, HC3, PB3	15	1
4	DB4, HC4, PB4	15	2
5	DB5, HC5, PB5	20	1
6	DB6, HC6, PB6	20	2

Here, our whisker sensor explored 3 sets of textures. Each set represents a specific type of surface pattern (see Fig. 3B): Dimple bumps (DB), Honeycomb (HC) and Pyramid bump (PB). These textures are parameterized by three measures: width (W), distance (D) from a pattern to the adjacent one and height (H). For simplification, W and D are set equal to each other in all samples (hereafter, WD is used to present both metrics). Each texture collection has 6 different textured plates (numbered from 1 to 6) whose geometrical parameters are listed in Table 1. In summary, a total of 18 samples were designed and 3D printed using ABS-based filament in such a way those pattern elements are centered along the plate.

B. EXPERIMENTAL SETUP FOR DATA COLLECTION

A series of sweeping experiments were implemented using the setup shown in Fig. 3A. Two motorized linear stages (Suruga Seiki, Japan) were set up orthogonally to carry the whisker sensor (X-axis stage) and the texture plates (Y-axis stage). While the X stage is responsible to ensure the relative position of the whisker tip and the textured plate, the Y stage drives texture plates back and forth with constant velocity $v = 20$ mm/s for surface exploration. Both stages are controlled by a motor controller DS102 (Suruga Seiki, Japan). During the surface exploring process of the whisker, the strain output was recorded at a sampling rate of 100 Hz by EDX-15A connected with a bridge box UI-54A-120, Kyowa, Japan, in synchronization with the movement of stages. Strain output in $\mu m/m$ from the measuring device is converted by the equation: $\varepsilon = \frac{\varepsilon_{read}}{GF} \times 10^{-3}$, where: ε_{read} is read from the software and GF stands for the gauge factor provided by the vendor ($GF = 2.21 \pm 1\%$). Additionally, the air chamber was pressurized to the desired value of Q by a pneumatic actuation system comprising a solenoid valve VQO1211 (SMC Co., Japan) and a pressure control valve AS2211FE-01 within the mainstream. Thanks to this combination, desired levels of inner pressure Q were always ensured. This system is controlled by a microprocessor (Arduino MEGA 2560) with feedback from a digital pressure sensor ISE20A-R-M (SMC Co., Japan).

The following identical procedure was performed for every texture. Firstly, the chamber was given an initial condition equivalent to the inner pressure $Q_{init} = 100$ kPa as previously

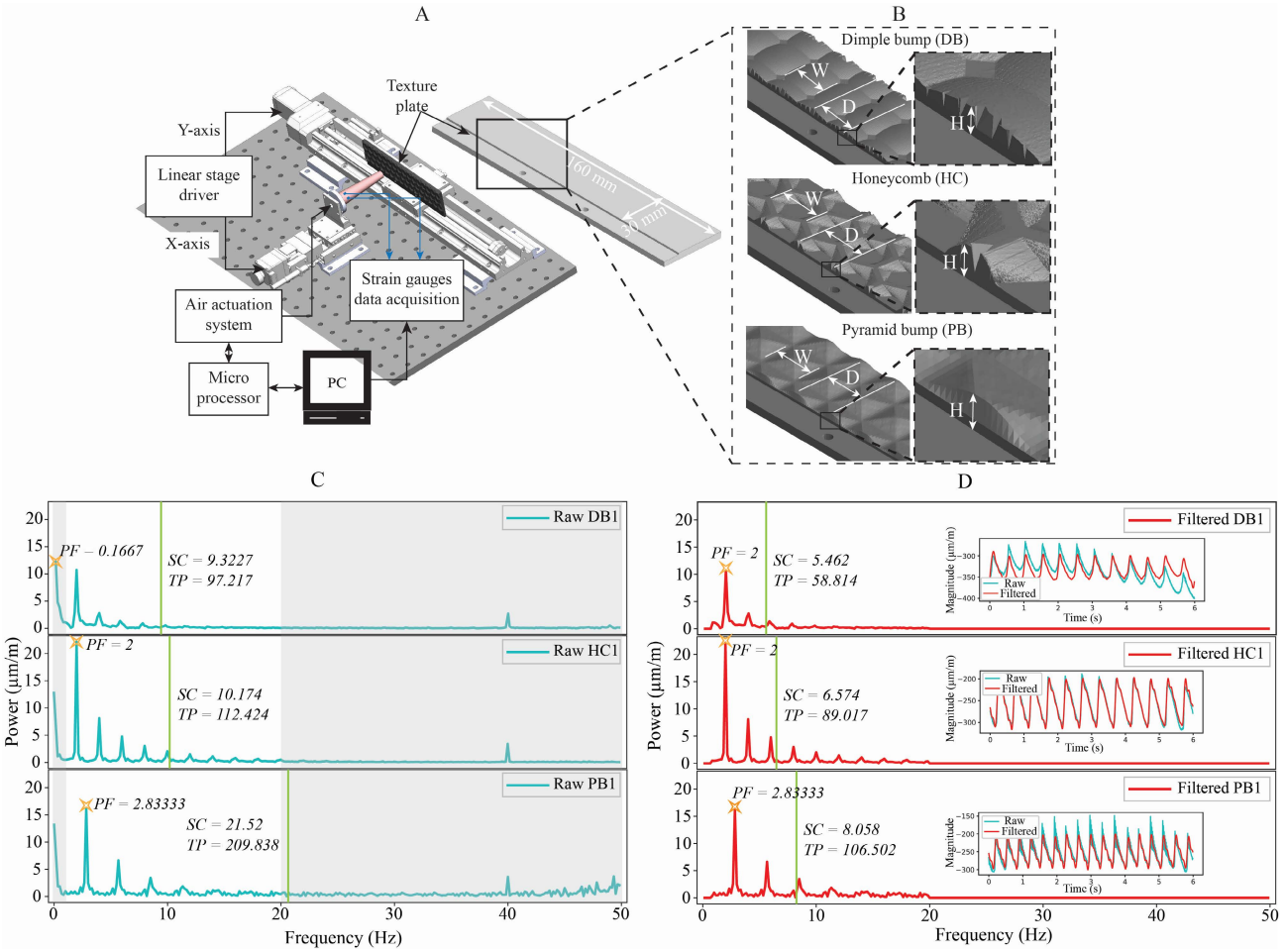

FIGURE 3. **(A) Experiment setup. (B)The texture plates are grouped in 3 different categories: Dimple Bump - DB, Honeycomb - HC and Pyramid bump - PB, which are attached to motorized linear stages for tactile exploration. Their geometry can be parameterized by three parameters: width (*W*), distance (*D*) from a pattern to the adjacent one and height (*H*). The morphology transformation is activated by an air actuation system under control of a micro processor. All measurement devices are managed by a desktop computer. (C) Three raw signal samples of DB1, HC1 and PB1 (in frequency domain) obtained by driving the intact whisker with constant velocity of 20 mm/s: The shaded area indicates the eliminated redundant frequency components. The yellow marker, green vertical line represent for *PF* and *SC*, respectively. (D) Respective power spectrum and converted signals in time-domain (inset graphs) after data processing as well as three texture features (*SC* (green lines), *TP* and *PF* (orange markers)) in such cases are also included.**

suggested in [1] and [2]. The test did not begin until the whisker tip reached the base of the texture plate. Then, a complete cycle of texture exploration is carried out as followed: a) sliding the texture plate forward for 160 mm (the plate length) at a preset speed of 20 mm/s. In the meantime, the response of S1 and S2 will be recorded within a time window of 6 seconds (*i.e.,* a 600 time-series of strain values) and labeled as forward data; b) repeating the same procedure for the backward direction. Note that a following sweeping session will start instantly after the whisker flicks over the texture plate (*i.e.,* no pre-bending). Here, 50 repeated cycles (*i.e.,* 25 forward and 25 backward datasets) were performed to create a database for texture classification.

C. FEATURE EXTRACTION FOR REGRESSION

Potential exploratory behaviors of a whisker sensor have been exploited for many purposes such as radial distance estimation [13], measuring geometrical attributes [23] and also texture discrimination [24]. Although up to date, the data processing method of rodent brains to extract the nature of a texture has not been fully understood, many approaches to biomimetic or artificial whiskers have shown that spectral analysis could prove significant texture-related information [25]. However, since we address a classification problem for variable textures (see Table 1), the spectral analysis may infer a wrong conclusion when there were differences in spectral phase [26]. Thus, texture discrimination based solely on frequency-amplitude spectrum is considered insufficient, resulting in the necessity of time-series data.

The signal spectrum in the frequency domain was obtained using Fast Fourier Transformation (FFT) over the data windows (see Fig. 3C-D). In details, three properties will be used as texture-related features: *Spectrum centroid* (*SC* - the green vertical line in Fig. 3C), *total power* (*TP*) of the spectrum and *predominant frequency* (*PF* - the yellow marker in Fig. 3C). Correspondences of the first two measures with

physical frequency and depth of bumps of the texture were previously established [27]. The last feature PF is the most powerful frequency component, thus, this signal is expected to capture the coupling between plate's driving speed and geometrical patterns of each texture. First of all, it is essential to eliminate redundant signal components that are independent of the texture geometry. We analyzed three samples of raw tactile data for DB1, HC1 and PB1 textures in the frequency domain (see Fig. 3C). We ascertain that unrelated frequency components located at very low frequencies up to 0.8333 Hz and from 20 Hz to 50 Hz (shaded area in Fig. 3C). As mentioned in [25], very-low-frequency components with large power correspond to bending effects of the whisker sensor during exploratory sweeping but are not related to the textured surface. On the other hand, high-frequency components are often found with very small power and they reflect less information about the texture. For example, the 40 Hz component has relatively high power (compared to its neighbors) due to layer-to-layer 3D-printing gap (approximately 0.5 mm). Hence, the residual signals (see Fig. 3D) will be eventually identified by low-pass and high-pass filtering components ranging from 0 Hz to 0.8333 Hz and 20 Hz to 50 Hz, respectively. Afterward, the spectrum centroid (SC) of the filtered spectrum is calculated as amplitude-weighted mean frequency:

$$SC = \frac{1}{N} \frac{\sum_{n=0}^{N-1} n \times \omega \times X(n)}{\sum_{n=0}^{N-1} X(n)}, \tag{7}$$

where $X(n)$ is magnitude or weighted frequency value, f is the width of each spectral bin, N is the dimension of frequency domain and n represents for bin number. The value of TP for each spectrum is as:

$$TP = \frac{1}{N} \sum_{n=0}^{N-1} X(n). \tag{8}$$

Temporal analysis is a subsequent step focusing on useful information in time-series signals that are inverse-transformed from filtered frequency spectra. More specifically, the average *positive maximum*[1] (APM - shown as red markers in Fig. 4A) signal peaks within a consecutive range of time (set to 0.3 s) were collected. In summary, for each strain gauge, we can draw out a feature vector $\boldsymbol{\Psi}_S^{4\times1}$ as shown below:

$$\boldsymbol{\Psi}_S^{4\times1} = [SC,\ TP,\ PF,\ APM]^T, \forall S \in [S1, S2]. \tag{9}$$

The combined feature vector is: $\boldsymbol{\Psi}^{8\times1} = \left[\boldsymbol{\Psi}_{S1}^{4\times1}\ \boldsymbol{\Psi}_{S2}^{4\times1}\right]$. Note that this feature vector is for strain data in a 6-second time window (either forward or backward).

[1] peaks correspond to whisker bending phase

D. CLASSIFICATION PROBLEMS AND SOLUTIONS

To fulfill the purpose of this study, we attempted to solve a multi-output classification problem, in which, outputs characterize separately texture types and geometrical dimensions of texture (WD and H). In terms of labeling for texture types, we apply One-Hot encoding approach [28] to categorize a texture by a 3×1 vector (notated as $\boldsymbol{C}$) of binary variables where a texture is ascribed to a specific element and set to "1", while the rest are *dummy* variables (*i.e.,* "0"). Vector $\boldsymbol{C}$ is equivalent to the probability of which texture category an arbitrary input data could belong to. Vector $\boldsymbol{C}$ combines with numerical values of WD and H to form the final observation vector for training and testing: $\boldsymbol{\Gamma}^{5\times1} = \left[\boldsymbol{C}^{3\times1}\ WD\ H\right]^T$.

We employed supervised Linear Regression (LR) learning algorithms. It should be noticed that the reference model was only trained with a subset of the database (80% of it) acquired from the intact whisker at initial pressure (*i.e.,* $Q_{init} = 100$ kPa). Consequently, performance assessment for any sensor configuration was compared against results of the remaining 20% testing data. Model training and data pre-processing were implemented with scikit-learn [29]. Database splitting for training and testing data was repeatedly conducted 10 times to demonstrate the independence of tactile sensing ability on random data selection. Therefore, experimental results (shown in the next section) are averaged over 10 trials.

The reliability of the above model will be challenged with two critical problems: (1) partially damaged whisker body and (2) encountering novel textures. Whilst most previous research focused on developing an often computationally expensive correction algorithm and manually adding new tactile data into the database, we rely on the interplay between the mechanics of the whisker morphology and external stimuli to form desired afferent sensory feedback to the central system. This interdependency is used to form a correction for strain data to maintain the sensing ability.

1) PROBLEM 1: TACTILE COMPENSATION FOR DAMAGED STRUCTURE

Tactile information is inferred from the consequences of physical interaction between soft bodies and the environment. Therefore, physical damages occurring to the sensor body lead to erroneous tactile information (e.g., mechanical strain) transmitted to the controller. Assuming the whisker sensor used for data collection is trimmed off by a certain length Δ (mm). The corresponding whisker's sensitivity to bending is increased proportionally to the fourth power of the outer diameter, making the strain output larger with the same stimuli (texture). Figure 4 pictures the signal magnitude in time domain and spectral power of three example cases: $\Delta = 0$ mm (intact), $\Delta = 1$ mm, and $\Delta = 5$ mm for texture HC1. One may observe the amplification of strain magnitude and power spectrum as Δ increases. This was also observed for the other texture features. In detail, except for the predominant frequency, other attributes (e.g., when

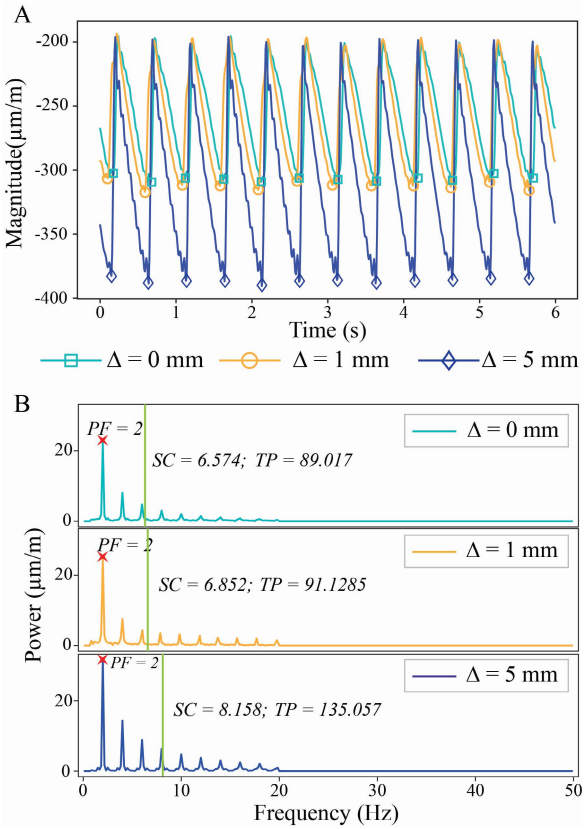

FIGURE 4. Comparison of tactile signal perceived from HC1 in time (figure (A) with *PM* peaks represented by markers) and frequency (figure (B) with *PF*, *SC* and *TP* features) domain among three prototypes: The original (light blue lines), 1 mm (orange lines) and 5 mm trimming length (dark blue lines).

$\Delta = 5$ mm) grow rapidly in comparison with those in the case $\Delta = 1$ mm. Significant impairment of tactile sensing is inevitable.

To prevent such circumstances, the whisker morphology should be varied in the manner of lowering the strain feedback (*i.e.,* sensitivity is decreased). According to Eq. 6, the strain value is inversely proportional to the material stiffness $E_2(Q)$ of the chamber, meanwhile, the contribution of geometrical parameters (*i.e.,* $\kappa(Q)$, δ_i $(i = 1, 2, 3)$) is not entirely unclear. Therefore, softening the chamber region (equivalent to reducing $E_2(Q)$) is the most promising solution. The experimental results reported in [1] and simulation results in [2] support this approach. The change in morphology was achieved by depressurizing the air chamber down to a proper value Q_c. To identify proper compensation pressure Q_c, we applied two methods:

1) The first method relies on the analytical model in section II-B. An optimal value for Q_c is obtained if the corresponding strain gauge output $\epsilon_b(Q_c)$ estimated by Eq. 6 does not differ significantly from the original ones in a same contact condition. We here searched for Q_c with contact ratio $a = 1$ (since the contact is occurred at the tip) and deflection $\delta(a)$ ranging up to 5 mm. Notice that this searching process was implemented for only S1 since its contribution to texture detection outperforms its counterpart (S2). Short expression for above method is as follows:

$$\varepsilon(Q_{init}) = \varepsilon_b(Q_c). \tag{10}$$

2) The second approach is inspired by searching adaptive behaviors of natural creatures throughout a "trial-and-error" process [30], [31]. Similarly, a trial-and-error could allow the whisker sensor to creatively discover compensatory solutions without an model. More specifically, the whisker sensors will gradually decrease inner pressure Q to maximize their sensing performance in spite of being damaged. Compensation results produced by these two methods will be compared for further clarification on pros and cons of resilient function based on an analytical approach.

2) PROBLEM 2: SURFACE ROUGHNESS ESTIMATION FOR UNKNOWN TEXTURE

Supervised learning techniques strongly depend on the quality and quantity of training data. Once an outlier appears, it is often necessary to collect related information and manually assign new labels to the training database for restarting the learning process (either online or offline). Otherwise, a degrading trend in classifier performance is unavoidable. However, the experimental data acquisition process is often burdensome in terms of time and cost. Not to mention the failure in control based on unfamiliar feedback from the environment will cause the failure of the robotic system. In this section, we tackle the problem when the classifier encounters a novel texture patterned similarly to DB, HC or PB, but with differences in geometrical dimensions.

To significantly improve the real-time roughness (*i.e.,* parameter H) recognition for unknown texture properties, our proposition is to actively change the sensor morphology (*i.e.,* changing from Q to Q_u) to enforce tactile information perceived from an unknown texture *close* to the one already included in the prior database. This *variation in morphology* could be referred equivalently to *differences in geometry* between them. Therefore, once the contribution of each state of sensor morphology to its perception is well-understood, we might be able to get knowledge about new textures with the help of solely morphological computation instead of any expensive-computational data analysis.

Let us assume that the strain signal reaches PM peaks (*i.e.,* whisker deflection δ is maximum) only when the whisker tip is sweeping over the highest points of the texture. In this scenario, the similarity in tactile data acquired from existed and unknown texture after calibration at these PM points (*i.e.,* $\varepsilon^e_{APM} = \varepsilon^u_{APM}$) yields following expression based on Eq. 6:

$$\frac{\delta^u_{max}(a)}{\delta^e_{max}(a)} = \frac{f^u(Q_u)}{f^e(Q_{init})}. \tag{11}$$

We argue that the ratio of whisker deflection in Eq. 10 (the left-hand side) is intuitively proportional to difference in height of the unknown texture and its counterpart. Moreover,

this measure is mathematically estimated through morphological computation (the right-hand side of Eq. 11).

IV. EXPERIMENTAL RESULTS AND EVALUATION

This section describes assessment methods and experiment results of the aforementioned methods for two research problems. Comparative experiments were conducted to demonstrate the robustness of the whisker sensor with adaptive morphology against physical damages at different levels. Subsequently, we tested the ability to discover the unknown texture's roughness upon previously trained textures.

A. EVALUATION METHODS

The evaluation session mainly focuses on two following criteria: the ability to, (a) successfully identify the correct texture types; and (b) precisely estimate all geometrical dimensions of the texture patterns. On one hand, the texture type prediction depends on which element in the vector $\boldsymbol{C}$ has the smallest deviation from the nominal value "1", *i.e.,* this is equivalent to the texture having the highest probability given the data sample. Additionally, this gap is also a measure to give an assessment on the reliability of texture prediction (shorten as *RTP*). On the other hand, estimations of geometrical parameters (*WD* and *H*) are validated by Root Mean Squared Error (RMSE) between estimated values and ground-truth values.

B. EXPERIMENT RESULTS

1) PROBLEM 1: TACTILE COMPENSATION FOR DAMAGED STRUCTURE

This section implements a comparative study of the classification performance of the whisker sensor being trimmed with that of the intact one in two scenarios: before and after tactile compensation. In turn, two showcases of [1, 5] mm cut-off length were studied. Firstly, it is necessary to identify the compensation pressure value Q_c for each case. The first method based on Eq. 9 suggests the proper values for Q_c are [94, 48] kPa, respectively for the two above cases. For the intact whisker (*i.e.,* $\Delta = 0$ mm and $Q = 100$ kPa), a high averaged success rate for texture type prediction is plotted in confusion matrix shown in Fig. 5. Figure 7 reports the texture characterization accuracy through *RSME* of three parameters *RTP*, *WD* and *H* and their standard deviation (SD). On contrary, texture classification results accomplished by broken whiskers have witnessed a significant decrease as the cut-off body length is increased as expected from Fig. 4. At the first glance, both trimmed whisker prototypes still retain the capability to correctly identify texture type, *i.e.,* the *RSME* of *RTP* in the case of $\delta = 1$ mm and $\delta = 5$ mm are approximately 0.2 and 0.4, respectively. However, these values are significantly larger than that of the intact whisker (around 0.1). This tendency remains true with that of *H* and even amplified for *WD*. Even far worse performance was implemented by the 5 mm shorten whisker. These results once again show that fragility could bring tremendous disability

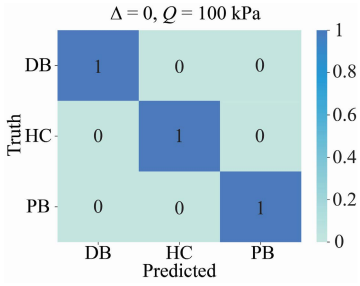

FIGURE 5. Confusion matrix of texture classifier for the case of intact whisker at its initial condition.

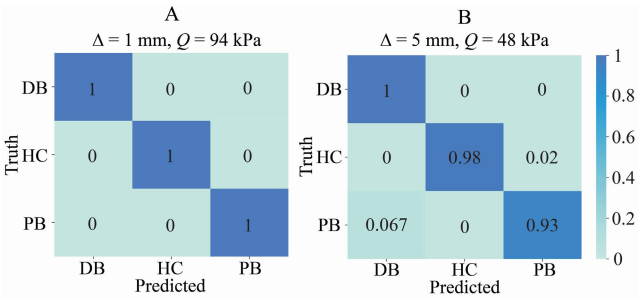

FIGURE 6. Confusion matrices of texture classifier for the case of broken whiskers with varied cut-off length: (A) $\Delta = 1$ mm and (B) $\Delta = 5$ mm.

to robot operation no matter how easy the task is. Corresponding actions to change the whisker's morphology (*i.e.,* lowering initial pressure Q_{init} down to compensation value Q_c) were activated to overcome the degrading in classification results. To identify proper values for Q_c, we first rely on the analytical model (method 1). Similar effort done in [1] suggested a reduction of the inner pressure down to 94 kPa and 48 kPa to achieve compensated states for the whisker with $\Delta = [1, 5]$ mm, respectively. The compensation results are summarized in Fig. 7. Only a slight improvement is observed for the case of 1 mm cut-off length, while a relatively substantial enhancement in texture classifying with the 5 mm cut-off whisker sensor is recognized. However, their performances are still far from what the intact whisker could achieve with a perfect body. The above results demonstrate the feasibility of tactile compensation ability against critical damages in structure based on morphological change. Since the overall sensing performance was not 100 percent recovered to the original state, it suggests that morphological transformation strategies tailored from the analytical model might not be optimal.

The trial-and-error processes (method 2) for searching for better morphology states were also executed. In detail, the broken whisker sensor will be tested its sensing ability within a decreasing range of pressure Q, with a step of 10 kPa until the sensing performance converges. Figure 8 illustrates the outcome of this approach. At first glance, the compensation performances for both damage cases apparently started to converge within the pressure range $90 - 80$ kPa and $40 - 30$ kPa when $\Delta = 1$ and 5 mm, respectively. This fact is reflected in *RMSE* of all interested indicators (see Fig. 7). Interestingly, these observations also narrow down the region

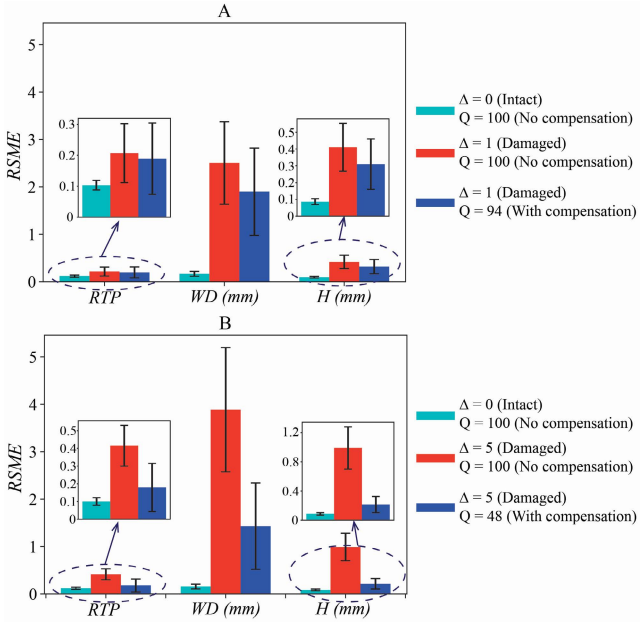

FIGURE 7. Accuracy comparison in texture characterization of the intact whisker sensor ($\Delta = 0$, $Q = 100$ kPa) and the broken whisker with different cut-off length and compensation states: (A) $\Delta = 1$ mm and (B) $\Delta = 5$ mm.

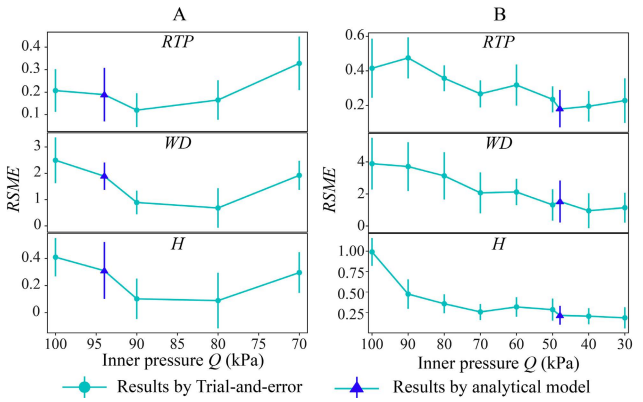

FIGURE 8. Evaluation of tactile compensation performance for broken whiskers with: (A) $\Delta = 1$ mm, $Q_c = 100 - 70$ kPa and (B) $\Delta = 5$ mm, $Q_c = 100 - 30$ kPa.

where the optimal sensor morphology can be found to recover malfunction in tactile sensing due to physical damages.

2) PROBLEM 2: SURFACE ROUGHNESS ESTIMATION FOR UNKNOWN TEXTURE

The results shown in the previous section have demonstrated that a tactile sensor could still achieve good classification and identification ability even, *i.e.,* when its body is critically damaged, thanks to online adaptive morphology. This section tackles another common issue for any classifier when they encounter unprecedented texture leading regression classifier to adverse outcomes.

To verify the solution described in Section III-D2, this session examined a new DB texture indexed as DB7 whose geometrical parameters are $WD = 15$ mm and $H = 1.5$ mm. The first step is to decide which existing textures will be paired up with DB7 for a comparative study. Specifically, it is reckoned as a good match-up when they

1) have a small deviation in terms of tactile information produced in time and frequency domain, or in other words, the dissimilarity in pattern dimensions is smallest, and
2) allow successful sensitivity calibration within the transformability limit of the body and sensitive range of the strain gauge.

TABLE 2. List of textures and their geometrical dimensions.

Comparative pair	Q_u (kPa)	$\delta^u_{max}(a)/\delta^e_{max}(a)$*
DB7 vs DB3	59	1.215
DB7 vs DB4	127	0.789

*Estimated from Eq. 11

As a result, for this experiment, the closest pairs for DB7 are DB3 or DB4 textures. Then, in order to predict the roughness of DB7, we adjust the whisker's sensitivity so as to receive similar strain gauge's outputs (ϵ^u_{APM}) with that of DB3 and DB4 (ϵ^e_{APM}) when the whisker reaches the texture's highest points. The ratio of max deflection between two contesters ($\delta^e_{max}(a)$ and $\delta^u_{max}(a)$) can be attributed to the difference in height among them and mathematically calculated using Eq. 11. Table 2 reports the results of roughness estimation based on the above hypothesis in comparison with real values acquired from experiments.

The ratio 1.215 and 0.789 indicates that, due to the difference in H, interaction with DB7 would most likely deflect the whisker sensor 1.215 times larger and 0.789 times smaller than that of DB3 and DB4, respectively. Furthermore, these ratios are not too far off from the real values (1.1875 and 0.869, respectively). They do not necessarily represent the ratio of unforeseen texture roughness but a measure to give us a rough estimate of it in general. If the correlation between maximum deflection of the whisker and texture peaks is given we could more precisely quantify the estimated value of H.

V. DISCUSSION AND CONCLUSION

Firstly, this paper extends our previous works to deal with structural damages in the soft whiskered tactile sensor in a more challenging sensing task (texture discrimination). Despite being trimmed, the tactile perception of the sensory whisker still remains unaffected, thanks to the tactile compensation method via adaptive sensor morphology. In detail, we demonstrated changing properly the whisker body by air regulation in the chamber would "pre-processing" the incorrect sensor response (mechanical strain) toward the right classification of the texture in sensor space. This hypothesis was tested with two: broken body length $\Delta = 1$ mm and $\Delta = 5$ mm. Two approaches are applied to discover the correct compensatory morphology, one is based on an analytical model first introduced in [1] and the other is inspired by a trial-and-error process that is widely used in natural creatures. Evaluation results shown in Fig. 7 have proved the feasibility of both approaches in enhancing the feature-based identification of texture plates for the broken whisker prototypes.

However, experimental results of compensation performance based on the analytical model showed a gap to those attained by the trial-and-error method (see Fig. 7). This can be explained by the fact that the model summarized in Section III-B does not take into account all dynamic aspects of physical interaction between the texture plates and the whisker sensor. The most obvious missing is friction force which temporally affects the whisker bending, then the strain gauge responses. Not to mention other factors such as sweeping velocity, and tactics for tactile exploration (passive or active) have been also testified with rodent whiskers as well as robotic whiskers to have an influence on overall distinguishing perception [32]. Instead of being the main provider for compensation actions, the analytical model should rather be utilized to orient other seeking techniques such as reinforcement learning (an advanced form of trial-and-error) toward feasible regions faster.

Secondly, we also tried to take advantage of adaptable sensor morphology to augment tactile discriminability with newly encountered environments. While many researchers aim at vast labeled data collection serving for the advancement of classifier models, which is sometimes unaffordable, we hypothesized that: variation of sensor morphology to calibrate tactile data perceived from novel objects close to prior-learned data would shed a light on geometrical differences or similarities. Section IV-B2 showcases this idea with a rough characterization for the texture height (H) of texture DB7 upon the most-similar textures (DB3 and DB4) in database. Another important point is the odd tactile information is filtered close to familiar ones so that the controller could still apply its pre-programmed policies without online re-specifying a new plan.

Whilst the ability to strengthen tactile perception based on morphological change is promising, it must be admitted that overall tactile sensing performance after compensation still has a gap with its original state. We argue that tactile resilience is limited to shape-changeable space and included actuation modes for our current design but could be improved. Therefore, the most straightforward solution is to increase locally controllable degrees of freedom throughout the deformable body. For example, advances in 3D printing could allow complex custom arrangements of air chambers within the body. However, design optimization is another consideration. That poses a potential future work where an efficient, automated simulation pipeline for seeking an optimal design that facilitates fabrication process and morphology control, and compensatory behaviors for a given task. We plan to expand the proposed idea to other soft robotic mechanisms with similar structures and at high risk of being damaged, such as soft fingers. Even beyond that, the method of adaptive morphology could be leveraged to meet the demand in other aspects of robotics once the relationship between morphology and function/problem is given. For instance, laparoscopes used in Minimally Invasive Surgery (MIS) could potentially benefit from tactile sensors with variable morphology [33]. In addition to providing tactile sensation which is a commonly known drawback of MIS, variable morphology allows controlling with adaptive sensory feedback toward more safe interaction with different types of organs. This direction is expected to push the role of sensor morphology beyond being a crucial part of constituting the sensory-actuator network.

ACKNOWLEDGMENT

The authors would like to thank Quan Khanh Luu for his useful advice on the supervised learning methods. Conclusions in this article are supported by raw data available at: (https://github.com/Ho-lab-jaist/Whisker-sensor.git).

REFERENCES

[1] N. H. Nguyen and V. A. Ho, "Mechanics and morphological compensation strategy for trimmed soft whisker sensor," *Soft Robot.*, vol. 9, no. 1, pp. 135–153, Feb. 2022.

[2] N. H. Nguyen and V. A. Ho, "Tactile compensation for artificial whiskered sensor system under critical change in morphology," *IEEE Robot. Autom. Lett.*, vol. 6, no. 2, pp. 3381–3388, Apr. 2021.

[3] E. G. Daylight, "Towards a historical notion of 'Turing—The father of computer science,"' *Hist. Philosophy Log.*, vol. 36, no. 3, pp. 205–228, Jul. 2015.

[4] H. J. Caulfield and S. Dolev, "Why future supercomputing requires optics," *Nature Photon.*, vol. 4, no. 5, pp. 261–263, 2010.

[5] L. M. Adleman, "Molecular computation of solutions to combinatorial problems," *Science*, vol. 266, no. 5187, pp. 1021–1024, 1994.

[6] R. Pfeifer and G. Gómez, "Morphological computation—Connecting brain, body, and environment," in *Creating Brain-Like Intelligence*. Berlin, Germany: Springer-Verlag, 2009, pp. 66–83.

[7] D. Shah, B. Yang, S. Kriegman, M. Levin, J. Bongard, and R. Kramer-Bottiglio, "Shape changing robots: Bioinspiration, simulation, and physical realization," *Adv. Mater.*, vol. 33, no. 19, May 2021, Art. no. 2002882.

[8] D. S. Shah, J. P. Powers, L. G. Tilton, S. Kriegman, J. Bongard, and R. Kramer-Bottiglio, "A soft robot that adapts to environments through shape change," *Nature Mach. Intell.*, vol. 3, no. 1, pp. 51–59, Jan. 2021.

[9] H. X. Trinh, Y. Iwamoto, V. A. Ho, and K. Shibuya, "Localization of sliding movements using soft tactile sensing systems with three-axis accelerometers," *Sensors*, vol. 19, no. 9, p. 2036, Apr. 2019.

[10] T. Umedachi, T. Kano, A. Ishiguro, and B. A. Trimmer, "Gait control in a soft robot by sensing interactions with the environment using self-deformation," *Roy. Soc. Open Sci.*, vol. 3, no. 12, Dec. 2016, Art. no. 160766.

[11] V. Anh Ho, H. Yamashita, Z. Wang, S. Hirai, and K. Shibuya, "Wrin'Tac: Tactile sensing system with wrinkle's morphological change," *IEEE Trans. Ind. Informat.*, vol. 13, no. 5, pp. 2496–2506, Oct. 2017.

[12] S. G. Nurzaman, U. Culha, L. Brodbeck, L. Wang, and F. Iida, "Active sensing system with *in situ* adjustable sensor morphology," *PLoS ONE*, vol. 8, no. 12, Dec. 2013, Art. no. e84090.

[13] N. H. Nguyen, T. D. Ngo, D. Q. Nguyen, and V. A. Ho, "Contact distance estimation by a soft active whisker sensor based on morphological computation," in *Proc. 8th IEEE RAS/EMBS Int. Conf. Biomed. Robot. Biomechatronics (BioRob)*, Nov. 2020, pp. 322–327.

[14] C. Lucarotti, M. Totaro, A. Sadeghi, B. Mazzolai, and L. Beccai, "Revealing bending and force in a soft body through a plant root inspired approach," *Sci. Rep.*, vol. 5, no. 1, p. 8788, Aug. 2015.

[15] A. A. Blandin, I. Bernardeschi, and L. Beccai, "Biomechanics in soft mechanical sensing: From natural case studies to the artificial world," *Biomimetics*, vol. 3, no. 4, p. 32, Oct. 2018.

[16] K. Sugiura, H. Kawakami, and O. Katai, "Simultaneous design of the sensory morphology and controller of mobile robots," *Electr. Eng. Jpn.*, vol. 172, no. 1, pp. 48–57, Jul. 2010.

[17] L. Van Duong and V. A. Ho, "Large-scale vision-based tactile sensing for robot links: Design, modeling, and evaluation," *IEEE Trans. Robot.*, vol. 37, no. 2, pp. 390–403, Apr. 2021.

[18] J. Hughes, L. Scimeca, P. Maiolino, and F. Iida, "Online morphological adaptation for tactile sensing augmentation," *Frontiers Robot. AI*, vol. 8, Jul. 2021, Art. no. 665030.

[19] Z. Yu, S. M. H. Sadati, H. Hauser, P. R. N. Childs, and T. Nanayakkara, "A semi-supervised reservoir computing system based on tapered whisker for mobile robot terrain identification and roughness estimation," *IEEE Robot. Autom. Lett.*, vol. 7, no. 2, pp. 5655–5662, Apr. 2022, doi: 10.1109/LRA.2022.3159859.
[20] F. Vollrath, "Leg regeneration in web spiders and its implications for orb weaver phylogeny," *Bull. Brit. Arachnolog. Soc.*, vol. 8, pp. 177–184, Jan. 1990.
[21] F. Vollrath, "Lyriform organs on regenerated legs of the garden cross spider," *Bull. Brit. Arachnolog. Soc.*, vol. 10, pp. 115–118, Jan. 1995.
[22] A. Holtmaat and K. Svoboda, "Experience-dependent structural synaptic plasticity in the mammalian brain," *Nature Rev. Neurosci.*, vol. 10, no. 9, pp. 647–658, Sep. 2009.
[23] H. Emnett, M. Graff, and M. Hartmann, "A novel whisker sensor used for 3D contact point determination and contour extraction," in *Robotics: Science and Systems*, H. Kress-Gazit, S. S. Srinivasa, T. Howard, and N. Atanasov, Eds. Pittsburgh, PA, USA: Carnegie Mellon Univ., Jun. 2018.
[24] Z. Yu, S. Perera, H. Hauser, P. R. N. Childs, and T. Nanayakkara, "A tapered whisker-based physical reservoir computing system for mobile robot terrain identification in unstructured environments," *IEEE Robot. Autom. Lett.*, vol. 7, no. 2, pp. 3608–3615, Apr. 2022.
[25] J. Hipp, E. Arabzadeh, E. Zorzin, J. Conradt, C. Kayser, M. E. Diamond, and P. König, "Texture signals in whisker vibrations," *J. Neurophysiol.*, vol. 95, no. 3, pp. 1792–1799, Mar. 2006.
[26] P. Giguere and G. Dudek, "A simple tactile probe for surface identification by mobile robots," *IEEE Trans. Robot.*, vol. 27, no. 3, pp. 534–544, Jun. 2011.
[27] C. W. Fox, B. Mitchinson, M. J. Pearson, A. G. Pipe, and T. J. Prescott, "Contact type dependency of texture classification in a whiskered mobile robot," *Auto. Robots*, vol. 26, no. 4, pp. 223–239, May 2009.
[28] S. L. Harris and D. Harris, "3—Sequential logic design," in *Digital Design and Computer Architecture*, S. L. Harris and D. Harris, Eds. San Mateo, CA, USA: Morgan Kaufmann, 2022, pp. 106–169.
[29] F. Pedregosa, G. Varoquaux, A. Gramfort, V. Michel, B. Thirion, O. Grisel, M. Blondel, A. Müller, J. Nothman, G. Louppe, P. Prettenhofer, R. Weiss, V. Dubourg, J. Vanderplas, A. Passos, D. Cournapeau, M. Brucher, M. Perrot, and E. Duchesnay, "Scikit-learn: Machine learning in Python," *J. Mach. Learn. Res.*, vol. 12, pp. 2825–2830, Oct. 2012.
[30] K. Chatzilygeroudis, V. Vassiliades, and J.-B. Mouret, "Reset-free trial-and-error learning for robot damage recovery," *Robot. Auton. Syst.*, vol. 100, pp. 236–250, Feb. 2018.
[31] A. Cully, J. Clune, D. Tarapore, and J.-B. Mouret, "Robots that can adapt like animals," *Nature*, vol. 521, no. 7553, pp. 503–507, 2015.
[32] M. Oladazimi, W. Brendel, and C. Schwarz, "Biomechanical texture coding in rat whiskers," *Sci. Rep.*, vol. 8, no. 1, p. 11139, Dec. 2018.
[33] N. Bandari, J. Dargahi, and M. Packirisamy, "Tactile sensors for minimally invasive surgery: A review of the state-of-the-art, applications, and perspectives," *IEEE Access*, vol. 8, pp. 7682–7708, 2020.

NHAN HUU NGUYEN (Member, IEEE) received the bachelor's degree in mechanical engineering from The University of Da Nang—University of Science and Technology, Vietnam, in 2015, the master's degree from the Ming Chi University of Science and Technology, Taiwan, in 2017, and the Ph.D. degree in robotics from the Advanced Institute of Science and Technology (JAIST), Japan, in 2022. He has been working as a Postdoctoral Researcher with the Soft Haptics Laboratories, JAIST. His research interests include exploiting complex physical interaction between deformable robots and the surrounding environment to enable novel functionalities, such as tactile sensing or facilitate learning and controlling tasks.

HELMUT HAUSER (Member, IEEE) received the B.Sc. and M.Sc. degrees in electrical engineering and control theory and the Ph.D. degree in telematics/robotics from the University of Technology Graz, Austria. He is currently an Associate Professor in robotics with the University of Bristol and the Bristol Robotics Laboratory. He is also the Director of the EPSRC Centre of Doctoral Training for Robotics and Autonomous Systems (FARSCOPE TU). He also leads the U.K.-RAS Strategic Task Group for Soft Robotics, which promotes Soft Robotics in U.K. His research interests include morphological computation and embodiment, especially in the context of soft robotics, understanding the underlying principles of how complex physical properties of biological systems are exploited to facilitate learning and controlling tasks, and how these principles can be employed to design better robots. He is serving as an Associate Editor for IEEE Robotics and Automation Letters and the *Journal of Soft Robotics*.

PERLA MAIOLINO (Member, IEEE) received the B.Eng. and M.Eng. degrees in robotics and automation and the Ph.D. degree in robotics from the University of Genoa. During her Ph.D. work, she carried out research on the development and integration of distributed tactile sensor for robots, developing new technological solutions for artificial robot skin (CySkin). CySkin Technology has been shown at the "Robots" Exhibition at the Science Museum in London. From October 2017 to September 2018, she joined the Biologically Inspired Robotics Laboratory (BIRL), University of Cambridge, pursuing research related to soft robotics and soft tactile perception. Currently, she is an Associate Professor and a member of the Oxford Robotic Institute, University of Oxford.

VAN ANH HO (Senior Member, IEEE) received the Ph.D. degree in robotics from Ritsumeikan University, Kyoto, Japan, in 2012.

He completed the JSPS Postdoctoral Fellowship, in 2013, before joining Advanced Research Center Mitsubishi Electric Corporation, Japan. From 2015 to 2017, he worked as an Assistant Professor with Ryukoku University, where he led a Laboratory on Soft Haptics. Since 2017, he has been joining the Japan Advanced Institute of Science and Technology for setting up the Laboratory on Soft Robotics. His current research interests include soft robotics, soft haptic interaction, tactile sensing, grasping and manipulation, and bio-inspired robots.

Dr. Ho is a member of The Robotics Society of Japan (RSJ). He was a recipient of 2019 IEEE Nagoya Chapter Young Researcher Award, Best Paper Finalists at IEEE SII, in 2016, and IEEE RoboSoft, in 2020. He is the General Co-Chair of 2023 IEEE/SICE International Symposium on System Integration (SII). He is serving as an Associate Editor for IEEE Transactions on Robotics, IEEE Robotics and Automation Letters, and *Advanced Robotics*.